Polina V. Stognii*, Dmitriy I. Petrov, Nikolai I. Khokhlov, and Igor B. Petrov

Simulation of seismic processes in geological exploration of Arctic shelf

DOI 10.1515/rnam-2017-0036
Received April 18, 2017; accepted October 2, 2017

Abstract: The paper presents the results of application of a grid-characteristic method to simulation of wave processes in media with linearly-elastic and acoustic layers on the example of seismic exploration of the Arctic shelf. The grid-characteristic method correctly describes the contact and boundary conditions. The results of numerical simulation are presented, the method is shown to be applicable to solution of seismic exploration problem on the Arctic shelf.

Keywords: Grid-characteristic method, numerical modelling, Arctic seismic prospecting.

MSC 2010: 65M25, 86A15

The Arctic shelf of the Russian Federation contains large deposits of hydrocarbons [5]. Currently, this region contains 594 detected oil fields and 159 gas fields. The initially recoverable reserves of oil in the Arctic zone are about 7.8 billion tons including 500 million tons on the shelf, the gas reserves are 65 billion m^3 including 10 billion m^3 on the shelf [5]. The estimates of reserves obtained earlier have to be refined for all hydrocarbon fields. One of the main challenges in estimation of the amount of mineral resources is caused by the different ice formations. For example, the Kara sea contains drifting ice almost all year round, the Pechersk and Barents seas contain icebergs and hummocks [8]. In this regard, solution of modelling problems for wave processes appearing on the Arctic shelf becomes rather important. [7, 24].

1 Determining equations

The equations describing expansion of waves in a linearly-elastic medium [23, 26] were presented, for example, in Love [20],

$$\rho \frac{\partial}{\partial t} \boldsymbol{v} = (\nabla \cdot \sigma)^T \tag{1.1}$$

$$\frac{\partial}{\partial t} \sigma = \lambda (\nabla \cdot \boldsymbol{v}) I + \mu (\nabla \otimes \boldsymbol{v} + (\nabla \otimes \boldsymbol{v})^T) \tag{1.2}$$

where ρ is the density of the material, $\boldsymbol{v}$ is the motion velocity, σ is the Cauchy stress tensor, λ and μ are the Lame parameters determining the properties of elastic material [28], I is the unit tensor, $\otimes$ is the operator of tensor product, t is the time. Equation (1.2) is Hooke's law differentiated with respect to time.

In order to simulate numerically the propagation of waves in sea water and in the oil-gas incorporation, we use the following acoustic system:

$$\rho \frac{\partial}{\partial t} \boldsymbol{v} = -\nabla p \tag{1.3}$$

$$\frac{\partial}{\partial t} p = -c^2 \rho (\nabla \boldsymbol{v}) \tag{1.4}$$

***Corresponding author: Polina V. Stognii,** Moscow Institute of Physics and Technology (State University), Institutskii per.9, Dolgoprudnyi 141700, Moscow region, Russia. E-mail: stognii@phystech.edu
Dmitriy I. Petrov, Nikolai I. Khokhlov, Igor B. Petrov, Moscow Institute of Physics and Technology (State University), Institutskii per.9, Dolgoprudnyi 141700, Moscow region; Scientific Research Institute of System Development, Nakhimovskii prospekt 36k1, Moscow 117218

where p is the pressure, v is the motion velocity, ρ is the density, c is the speed of sound in the ideal fluid, t is the time.

The velocity of longitudinal and transverse waves in the linearly-elastic medium is calculated by the formulas

$$c_p = \sqrt{\frac{\lambda + 2\mu}{\rho}}, \qquad c_s = \sqrt{\frac{\mu}{\rho}}. \tag{1.5}$$

2 Numerical method of calculation

Numerical solution of systems of equations (1.1), (1.2) and (1.3), (1.4) is performed with the use of a grid-characteristic method [11] allowing us to construct well-definite numerical algorithms for calculation of points at boundaries [21] and points lying on interfaces of two media with different densities and different Lame parameters.

System of equations (1.1), (1.2) can be represented in a matrix form (three motion equations, six rheological relations [11]). For the three-dimensional case this system has the form

$$\frac{\partial \mathbf{q}}{\partial t} + \mathbf{A}_1 \frac{\partial \mathbf{q}}{\partial x_1} + \mathbf{A}_2 \frac{\partial \mathbf{q}}{\partial x_2} + \mathbf{A}_3 \frac{\partial \mathbf{q}}{\partial x_3} = 0. \tag{2.1}$$

Here $\mathbf{q}$ is the vector consisting of three velocity components and six components of the symmetric stress tensor:

$$\mathbf{q} = \{v_1, v_2, v_3, \sigma_{11}, \sigma_{22}, \sigma_{33}, \sigma_{23}, \sigma_{13}, \sigma_{12}\}^T. \tag{2.2}$$

The method of splitting with respect to spatial coordinates is applied to equations (2.1), which results in the following three systems of one-dimensional equations:

$$\frac{\partial \mathbf{q}}{\partial t} = \mathbf{A}_j \frac{\partial \mathbf{q}}{\partial x_j}, \quad j = 1, 2, 3. \tag{2.3}$$

Each of these systems is hyperbolic and has a complete set of eigenvectors with real eigenvalues, therefore, each of them can be written as

$$\frac{\partial \mathbf{q}}{\partial t} = \boldsymbol{\Omega}_j^{-1} \boldsymbol{\Lambda}_j \boldsymbol{\Omega}_j \frac{\partial \mathbf{q}}{\partial x_j}. \tag{2.4}$$

Here $\boldsymbol{\Omega}_j$ is the matrix composed of eigenvectors, $\boldsymbol{\Lambda}_j$ is the diagonal matrix whose elements are the eigenvalues. For all coordinates the matrix $\boldsymbol{\Lambda}$ looks like

$$\boldsymbol{\Lambda} = \mathrm{diag}\{c_1, -c_1, c_2, -c_2, c_2, -c_2, 0, 0, 0\} \tag{2.5}$$

where $c_1 = \sqrt{(\lambda + 2\mu)/\rho}$ is the longitudinal speed of sound in the medium, $c_2 = \sqrt{\mu/\rho}$ is the transverse speed of sound.

Changing the variables $\nu = \boldsymbol{\Omega}\mathbf{q}$, we split each of systems (2.4) into 9 independent scalar transfer equations:

$$\frac{\partial \boldsymbol{\nu}}{\partial t} + \boldsymbol{\Lambda} \frac{\partial \boldsymbol{\nu}}{\partial x} = 0. \tag{2.6}$$

One-dimensional transfer equations can be solved by the method of characteristics or by finite-difference schemes [13].

After all the components $\boldsymbol{\nu}$ have been transferred, we can reconstruct the solution, i.e.,

$$\mathbf{q}^{n+1} = \Omega^{-1} \nu^{n+1}. \tag{2.7}$$

Transfer equation (2.6) was solved by the grid-characteristic method based on Rusanov's scheme of the 3rd order of accuracy (see [14]):

$$\nu_m{}^{n+1} = \alpha_{-2} \nu_{m-2}{}^n + \alpha_{-1} \nu_{m-1}{}^n + \alpha_0 \nu_m{}^n + \alpha_1 \nu_{m+1}{}^n \tag{2.8}$$

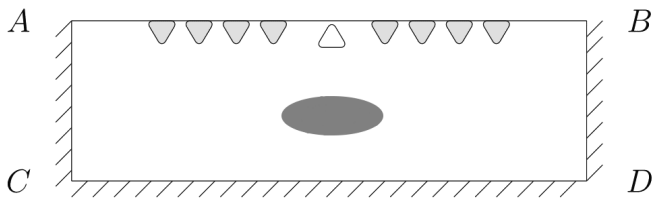

Figure 1: Schematic representation of the computational domain with indication of the boundaries.

where the coefficients α_{-2}, α_{-1}, α_0, and α_1 can be obtained from the condition of the 3rd order approximation of the scheme by expanding it into a Tailor series relative to, for example, the point $({x_m}^n)$. As the result, we get the following system of equations for the unknown coefficients α:

$$\alpha_{-2} + \alpha_{-1} + \alpha_0 + \alpha_1 = 1 \tag{2.9}$$

$$-2\alpha_{-2} - \alpha_{-1} + \alpha_1 = -\sigma \tag{2.10}$$

$$4\alpha_{-2} + \alpha_{-1} + \alpha_1 = \sigma^2 \tag{2.11}$$

$$-8\alpha_{-2} - \alpha_{-1} + \alpha_1 = -\sigma^3. \tag{2.12}$$

Here $\sigma = \lambda\tau/h$, where λ is the transfer rate, τ is the time integration step, h is the integration step in the coordinate.

The numerical solution was regularized with the use of the monotonicity criterion [14]. For the positive values $\lambda > 0$ this criterion is the following:

$$\min\{{v_m}^n, {v_{m-1}}^n\} \leqslant {v_m}^{n+1} \leqslant \max\{{v_m}^n, {v_{m-1}}^n\} \tag{2.13}$$

while for negative values $\lambda < 0$ the criterion is symmetric.

In the computations we used the following conditions for the boundary:

(1) $(\sigma\mathbf{n}) = 0$ for calculation of the free boundary, where $\mathbf{n}$ is the unit normal to the surface of the body, σ is the Cauchy stress tensor;
(2) absorption condition.

The general formulation of the direct problem of seismic exploration is presented in Fig. 1: the condition of free boundary is posed on the upper boundary AB, the absorption condition is posed on the lateral boundaries AC, BD and on the lower boundary CD. The white triangle on the boundary AB indicates a point source of seismic waves, grey triangles indicate receivers of the signal.

The calculation showed the ability to use the grid-characteristic method for simulation of wave processes on the Arctic shelf. This numerical method allows us to pose correct boundary conditions for the integration domain and on boundaries of calculation domains. The method takes into account the physical nature of the phenomenon, i.e., propagation of perturbations along characteristics.

3 Conditions on the interface of the liquid and rigid body

We consider the condition on contact boundaries between integration parts described by systems of equations (1.1), (1.2) and (1.3), (1.4). Denote these contacting domains by a and b, $\mathbf{n}_{ab}$ is the outer normal to the rigid body being the inner normal to the liquid [6]. The contact condition of free slipping on the interface of the boundaries a and b is the following:

$$\mathbf{n}_{ab} \cdot \boldsymbol{v}^{a,n+1} = \mathbf{n}_{ab} \cdot \boldsymbol{v}^{b,n+1} = \mathbf{V}^{n+1} \tag{3.1}$$

$$[\mathbf{n}_{ab}, \boldsymbol{\sigma}^{a,n+1} \cdot \mathbf{n}_{ab}] = [\mathbf{n}_{ab}, \boldsymbol{\sigma}^{b,n+1} \cdot \mathbf{n}_{ab}] = 0 \tag{3.2}$$

$$p^{b,n+1} = -(\boldsymbol{\sigma}^{a,n+1} \cdot \mathbf{n}_{ab}) \cdot \mathbf{n}_{ab}. \tag{3.3}$$

Condition (3.1) provides the equality of normal velocity components in the ideal liquid and rigid body, (3.2) represents the vanishing of the tangent component of the surface density of forces acting from the rigid body, (3.3) equates the normal component of the surface density of forces from the rigid body to the pressure in the ideal liquid.

The velocity vector $\mathbf{V^{n+1}}$ is calculated so that conditions (3.1)–(3.3) hold, i.e.,

$$\mathbf{V}^{n+1} = \frac{1}{\rho_a c_{a2} + \rho_b c_{b2}} [\rho_a c_{a1} \boldsymbol{\upsilon}_a^{n+1(\text{in})} + \rho_b c_{b1} \boldsymbol{\upsilon}_b^{n+1(\text{in})} - (\boldsymbol{\sigma}_a^{n+1(\text{in})} - \boldsymbol{\sigma}_b^{n+1(\text{in})} \cdot \mathbf{n})] \cdot \mathbf{n} \tag{3.4}$$

The value $\boldsymbol{\upsilon}_a^{n+1(\text{in})}$ can be obtained in (3.4) in the same way as $\boldsymbol{\upsilon}_a^{n+1}$ for inner points. The value $\boldsymbol{\upsilon}_a^{n+1(\text{out})}$ is expressed from the boundary condition $\mathbf{Bq}^n = \mathbf{b}$

$$\boldsymbol{\upsilon}^{n+1(\text{out})} = (B\boldsymbol{\Omega}^{(\text{out})})^{-1}(\mathbf{b} - \mathbf{Bq}^{n+1(\text{in})}) \tag{3.5}$$

In (3.5), $\boldsymbol{\Omega}^{(\text{in})}$ and $\boldsymbol{\Omega}^{(\text{out})}$ are rectangular matrices composed of the columns of matrix $\boldsymbol{\Omega}^{-1}$ corresponding to characteristics coming in, or going out of the integration domain, respectively.

In order to describe the behaviour of the liquid, we use a mixed boundary condition with the given normal velocity component $\mathbf{V}_n$ and the tangent component $\mathbf{f}_\tau$ having the following form (see [12]):

$$\mathbf{f} = \mathbf{f}_\tau + \mathbf{n}(\rho c_1 \mathbf{V}_n + \mathbf{n} \cdot (\boldsymbol{\sigma}^{n+1(\text{in})} \cdot \mathbf{n} - \rho c_1 \boldsymbol{\upsilon}^{n+1(\text{in})})), \qquad \mathbf{f}_\tau = \mathbf{0}. \tag{3.6}$$

In (3.6), $\mathbf{f}$ is the total density of surface forces ($\boldsymbol{\sigma} \cdot \boldsymbol{n} = \boldsymbol{f}$). After that we use the following formulas for the given density of surface forces on the boundary $\mathbf{f}$:

$$\mathbf{q}^{n+1} = \mathbf{q}^{n+1(\text{in})} - \frac{c_1 \mathbf{z}^{n+1} - (c_1 - c_2)(\mathbf{z}^{n+1} \cdot \mathbf{n})\mathbf{n}}{\rho c_1 c_2} \tag{3.7}$$

$$\boldsymbol{\sigma}^{n+1} = \boldsymbol{\sigma}^{n+1(\text{in})} - \mathbf{z}^{n+1} \otimes \mathbf{n} - \mathbf{n} \otimes \mathbf{z}^{n+1} - \frac{(\mathbf{z}^{n+1} \cdot \mathbf{n})}{\lambda + 2\mu}(\lambda \mathbf{I} - 2(\lambda + \mu)\mathbf{n} \otimes \mathbf{n}). \tag{3.8}$$

Here $\mathbf{z}^{n+1} = \boldsymbol{\sigma}^{n+1(\text{in})} \cdot \mathbf{n} - \mathbf{f}$, $\mathbf{I} = \text{diag}(1, 1, 1)$.

For the rigid body we use the boundary condition with a given velocity $\mathbf{V}$ of the boundary

$$\boldsymbol{\upsilon}^{n+1} = \mathbf{V} \tag{3.9}$$

$$\boldsymbol{\sigma}^{n+1} = \boldsymbol{\sigma}^{n+1(\text{in})} - \rho[(\mathbf{n} \cdot \mathbf{g}^{n+1})((c_1 - 2c_2 - c_3)\mathbf{n} \otimes \mathbf{n} + c_3 \mathbf{I}) + c_2(\mathbf{g}^{n+1} \otimes \mathbf{n} + \mathbf{n} \otimes \mathbf{g}^{n+1})] \tag{3.10}$$

where $c_3 = \sqrt{\lambda^2/(\rho(\lambda + 2\mu))}$, $\mathbf{g}^{n+1} = \boldsymbol{\upsilon}^{n+1(\text{in})} - \mathbf{V}$.

4 Study of seismic wave fields in Northern seas in the presence of ice cover

We carried out numerical experiments for numerical solution of problems of seismic exploration on the Arctic shelf. We considered rheological models of ice, water, and soil. The ice was represented as an elastic plate of finite thickness on the water surface and was considered as a linearly-elastic deformable body because seismic pulses are so weak that deformations can be considered small. In this paper, the ice thickness was taken equal to 3 m although the thickness of the ice cover in the Arctic shelf area can be 2–2.5 m [8]. The developed algorithms and software allow us to calculate the ice fields of different thickness. We compared two models, i.e., with oil and gas layer and without it. In all calculations the spatial mesh size in x and y coordinates was taken equal to 5 m. The step in z direction in the ice cover was 0.5 m, in the water layer it was 1 m, and in the soil layer it was 5 m. The time step was taken equal to 10^{-4} s according to the Courant stability condition, 7 thousand steps in time were applied.

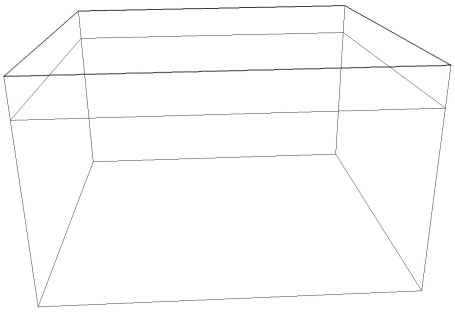

(a) Model with ice cover and without oil and gas layer.

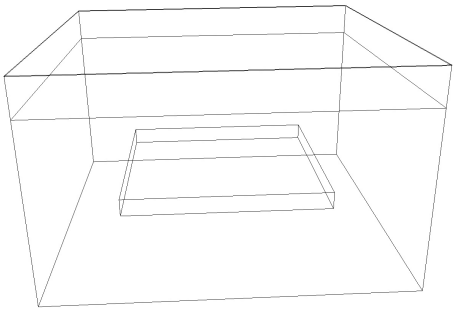

(b) Model with ice cover and oil and gas layer.

Figure 2: Schematic representation of models with ice cover at the initial time moment.

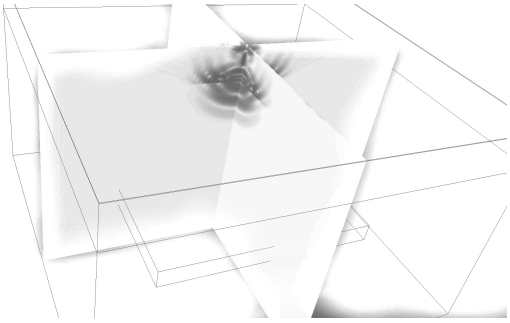

(a) Wave at the time moment 0.18 s in the following layers: ice cover, water.

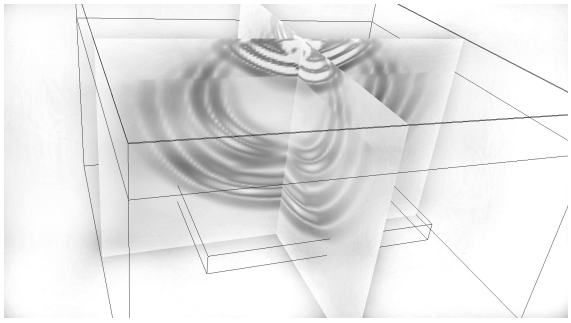

(b) Wave at the time moment 0.38 s in the following layers: ice cover, water, soil.

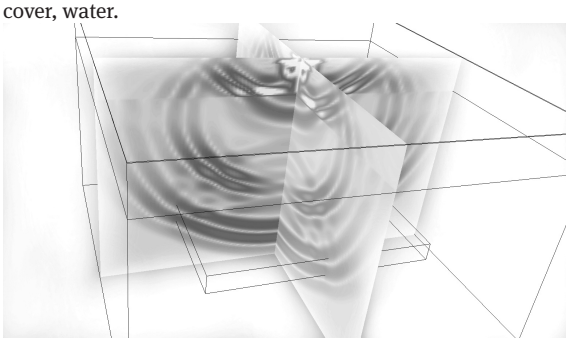

(c) Wave at the time moment 0.44 s in the following layers: ice cover, water, soil.

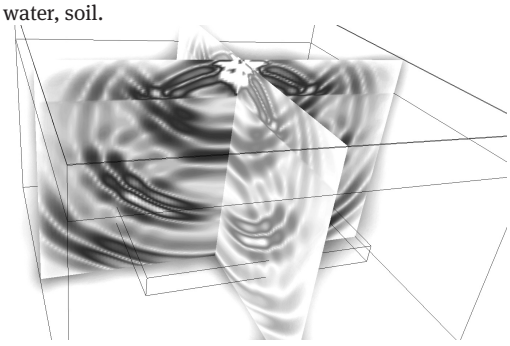

(d) Wave at the time moment 0.52 s in the following layers: ice cover, water, soil.

Figure 3: Wave patterns for models with ice cover at the different time moments.

We considered an ice layer with the density 917 kg/m^3, a water layer of thickness 200 m and density 1000 kg/m^3, a soil layer of thickness 1000 m and density 2100 kg/m^3. The size of the integration domain in x and y axes was 2000 by 2000 m. The oil and gas reservoir had the sizes 1200 m by 1200 m, the density of 1800 kg/m^3 and was located at the depth of 700 m under the ground. The longitudinal speed of sound in ice cover was taken equal to 3940 m/s, the transverse speed was 2493 m/s. The speed of sound in water was 1500 m/s. In the soil layer the transverse speed of sound was taken equal to 1875 m/s, the longitudinal one was 3000 m/s. The transverse speed of sound in the oil and gas layer was 2000 m/s, the longitudinal one was 2500 m/s. At the sides of the computational domain we posed non-reflecting boundary conditions [9].

The exposure was applied by a single Ricker source pulse located at the center of the computational domain on the surface of the ice cover. The receivers were located on the bottom at the center of the computational domain at the distance of 10 m from each other.

Schematic representation of models can be seen in Fig. 2: (a) the model with ice cover and without oil and gas layer; (b) the model with ice cover and oil and gas layer.

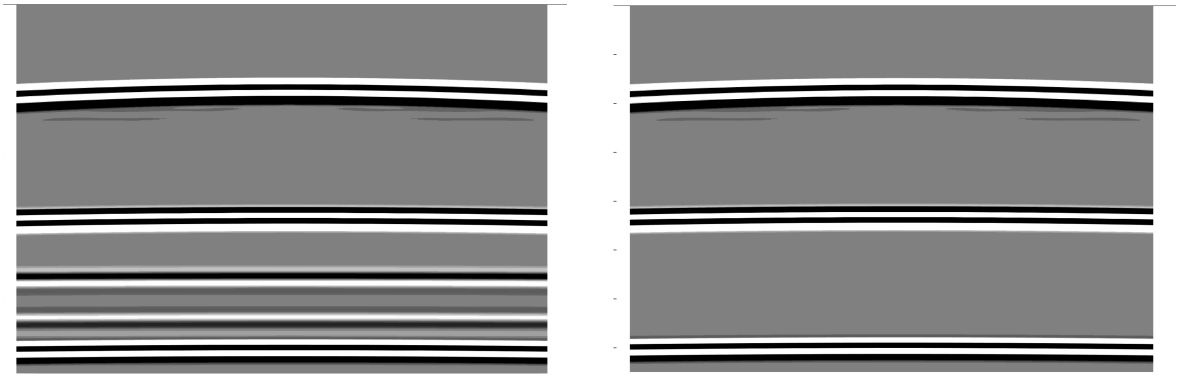

(a) Model with oil and gas layer.

(b) Model without oil and gas layer.

Figure 4: Typical seismograms to distinguish the situations of presence and absence of the oil and gas layer in models with ice cover.

It is difficult to represent the ice layer in the figure because its size is much smaller than that of water or soil. Figure 2 shows only the water, soil, and oil layers.

The wave patterns at the different time moments are presented in Fig. 3. In Fig. 3a the wave passes through the ice and water layers, in Fig. 3b the wave passes through the soil layer. In Figs. 3c and 3d the wave reaches the oil and gas layer and reflections from that layer are observed. Hereinafter the wave patterns were obtained using the software described in [25]. Figure 3c presents reflections from the oil and gas layer. It is seen that the ice layer does not affect the reflection from the inhomogeneity in the soil layer.

The z-axis seismograms for the given formulations of the problem are presented in Fig. 4. Upper parts of both Figs. 4a and 4b show feedback from the ice cover and water layer. Then, after a certain distance (namely, 200 m, which is the size of the water layer) both pictures show visible reflections from the soil layer. After that, in Fig. 4a we can see reflections from the oil and gas layer, but Fig. 4b has no such patterns, which corresponds to the conditions of the problem. The seismograms were obtained using the software described in [25].

Based on the obtained seismograms and wave patterns we can conclude that the ice cover does not essentially influence the appearance of reflections from the oil and gas layer.

5 Study of seismic wave fields in Northern seas in the presence of icebergs

In addition to ice cover, there are large ice formations, icebergs in Northern seas [2, 9, 10, 17]. We considered models with icebergs, water, and soil layers. In calculations we represented icebergs by rectangular ice structures with an area of 22500 m^2 and the keel depth of 30 m [15]. All parameters for the different layers (ice, water, soil, oil and gas), i.e., the density, speed of sound of longitudinal and transverse waves were taken the same as in the model with ice cover.

The size of the integration domain was 2000 by 2000 m. The thickness of the water layer was 200 m, for the soil layer it was 1000 m. An inhomogeneity of 1200 by 1200 m was located at the distance of 700 m under the ground.

We considered two formulations of the problem with different number of icebergs, namely, (1) one iceberg at a considerable distance from the point where the impact by the Ricker pulse originates (two models with oil and gas reservoir and without it, respectively); (2) two icebergs located at equal distances from the point of Ricker pulse disturbance (similarly, two models with oil and gas reservoir and without it). In both cases the icebergs were located at the distance of 750 m from the point of disturbance. Schematic representation of the four models can be seen in Fig. 5: (a) the model with one iceberg and oil and gas layer; (b) the model

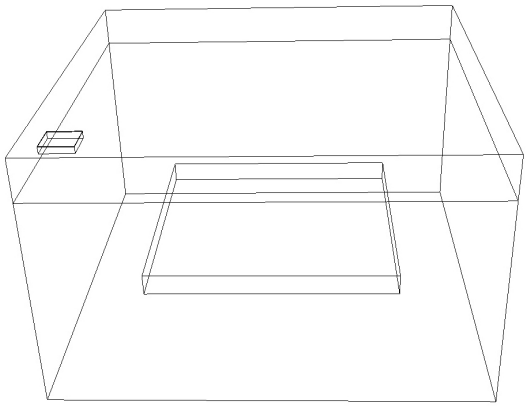

(a) Model with one iceberg and oil and gas layer.

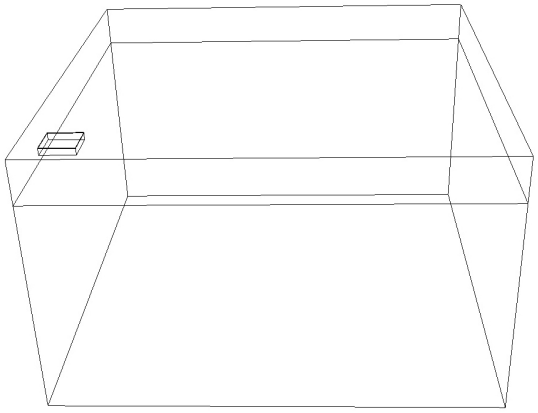

(b) Model with one iceberg and without oil and gas layer.

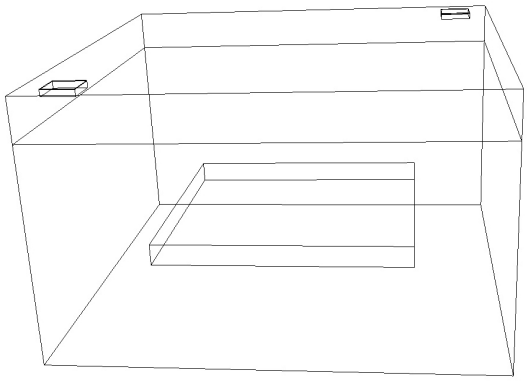

(c) Model with two icebergs and oil and gas layer.

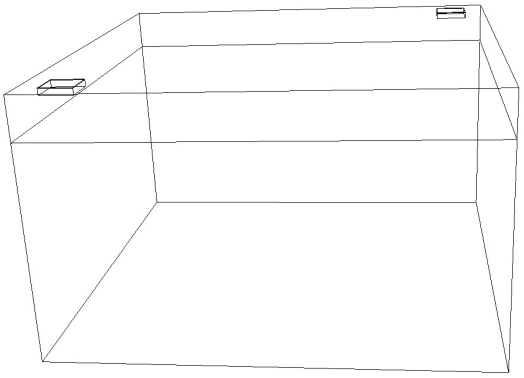

(d) Model with two icebergs and without oil and gas layer.

Figure 5: Schematic presentation of models with icebergs at the initial time moment.

with one iceberg and without oil and gas layer; (c) the model with two icebergs and oil and gas layer; (d) the model with two icebergs and without oil and gas layer.

The wave patterns for the problem with one iceberg are presented in Fig. 6. In Fig. 6a the wave passes through the water layer, in Fig. 6b the wave reaches the soil layer. In Figs. 6c and 6d the wave passes through the oil and gas layer and we can see reflections from it. In Fig. 6d the wave reaches the iceberg and we can see reflections from this ice inhomogeneity. Further we see in seismograms that the iceberg does not prevent the receipt of seismograms to get reflections from the oil and gas layer.

The wave patterns for the problem with two icebergs are presented in Fig. 7. In Fig. 7a the wave passes through the water layer, in Fig. 7b the wave reaches the soil layer; in Figs. 7c and 7d the wave passes through the oil and gas layer, we can see clear wave lines of reflection from it.

The z-axis seismograms for these formulations of the problem are presented in Fig. 8. Figures 8a and 8b present the readings of sensors for the case of one iceberg. One can see distinctions between the case of presence of the oil and gas layer and its absence in the form of additional reflections in the lower parts of figures. In the models with two icebergs one can also see similar distinctions in the presence/absence of the inhomogeneous layer (see Figs. 8c and 8d). The icebergs do not essentially affect the readings (seismological tracks) from the sensors because ice heterogeneities are located sufficiently far (750 m) from the point of action.

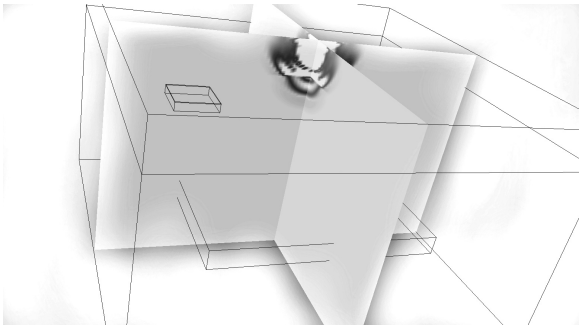

(a) Wave at time moment 0.15 s in the water layer.

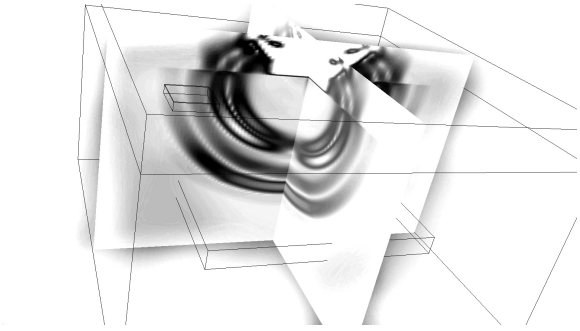

(b) Wave at time moment 0.35 s in the water and soil layers.

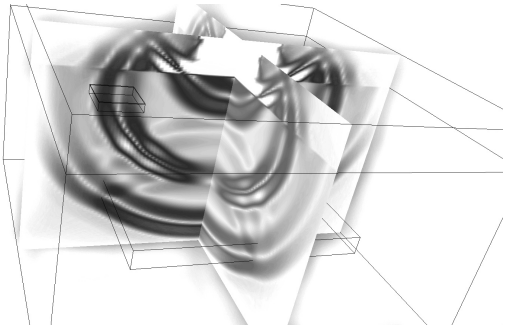

(c) Wave at time moment 0.45 s in the water and soil layers.

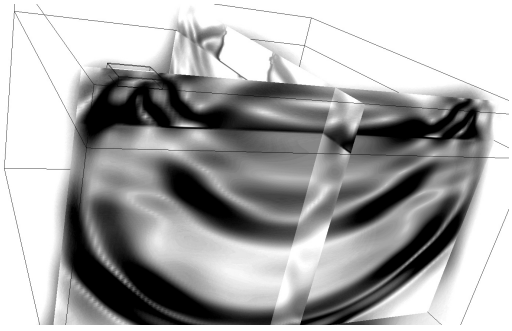

(d) Wave at time moment 0.8 s in the water and soil layers.

Figure 6: Wave patterns at the different time moments for the model with one iceberg.

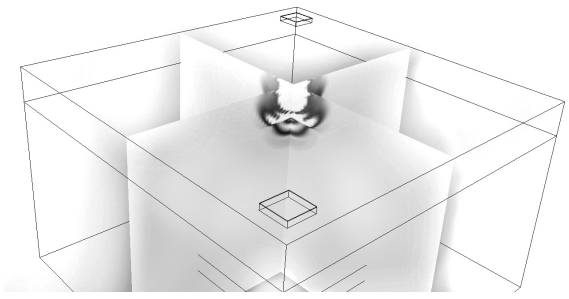

(a) Wave at time moment 0.15 s in the water layer.

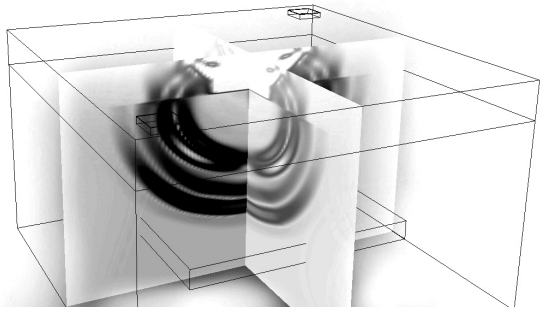

(b) Wave at time moment 0.35 s in the water and soil layers.

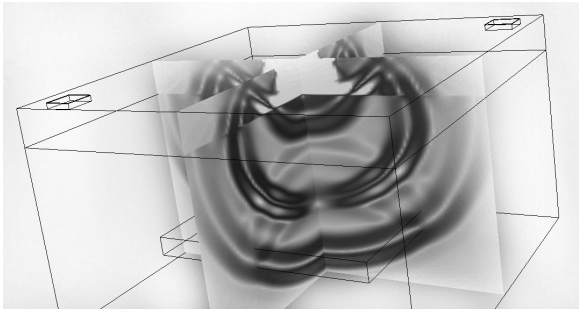

(c) Wave at time moment 0.45 s in the water and soil layers.

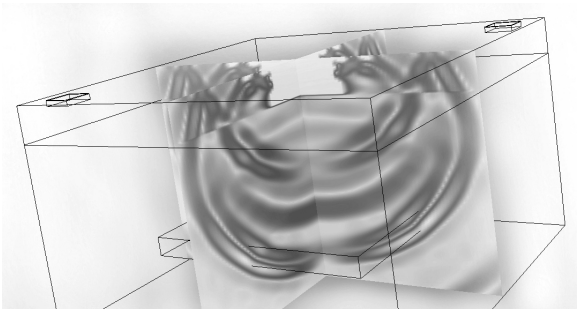

(d) Wave at time moment 0.6 s in the water and soil layers.

Figure 7: Wave patterns at the different time moments for the model with two icebergs.

(a) Model with one iceberg and oil and gas layer.

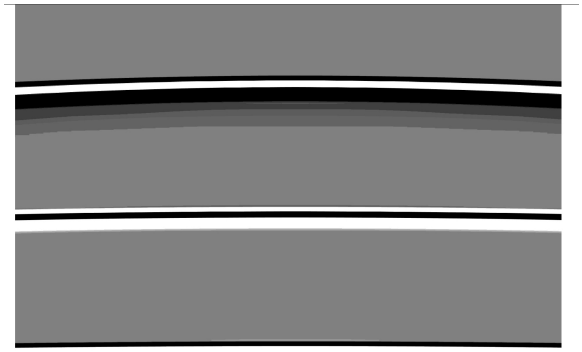

(b) Model with one iceberg without oil and gas layer.

(c) Model with two icebergs and oil and gas layer.

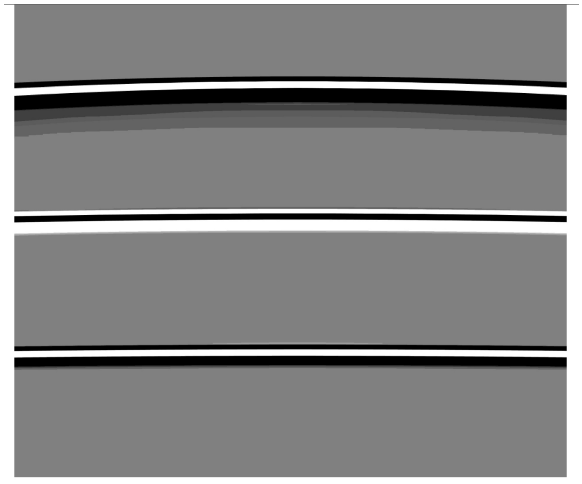

(d) Model with two icebergs and without oil and gas layer.

Figure 8: Typical seismograms to distinguish the situations of presence and absence of the oil and gas layer in models with icebergs.

6 Study of seismic wave fields in Northern seas in the presence of ice hummocks

Ice hummocks being big piles of ice debris appear in Northern seas [10] and their keels can reach the depth of 40–50 meters [29].

The model was formed by the water and soil layers. We compared models with the presence or absence of the oil and gas layer with the presence of a hummock in both cases and the model without oil and gas layer and hummock to study in detail reflections from the oil and gas layer and from the ice hummock. In our calculations the hummock was a set of ice structures with gaps filled with water. Usually, the keel of hummock has a triangular form, but the form shown in Fig. 9d may also occur [22]. In the calculations the keel depth was 50 m.

All the parameters (density, speed of sound) of the ice, water, soil, oil and gas layer were taken equal to the values from the model with ice cover.

The size of integration domain in calculations was 2000 by 2000 m. The thickness of the water layer was 200 m, for the soil layer it was 1000 m. An inhomogeneity of 1200 by 1200 m was located at the distance of 700 m under the ground.

The schematic presentation of the models is shown in Fig. 9: (a) the model with a hummock and without oil and gas layer; (b) the model with a hummock and oil and gas layer; (c) the model without a hummock and oil and gas layer; (d) the model of hummock.

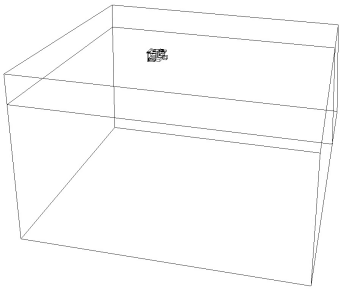

(a) Model with hummock and without oil and gas layer.

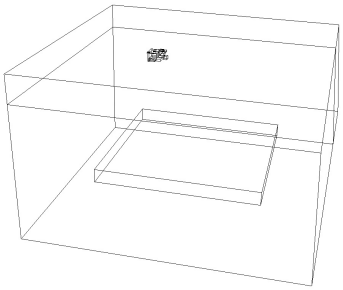

(b) Model with hummock and oil and gas layer.]

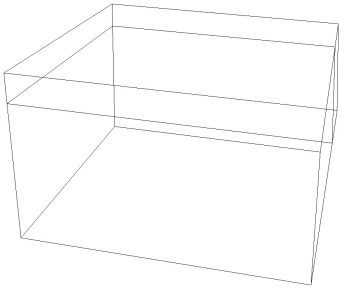

(c) Model without hummock and oil and gas layer.

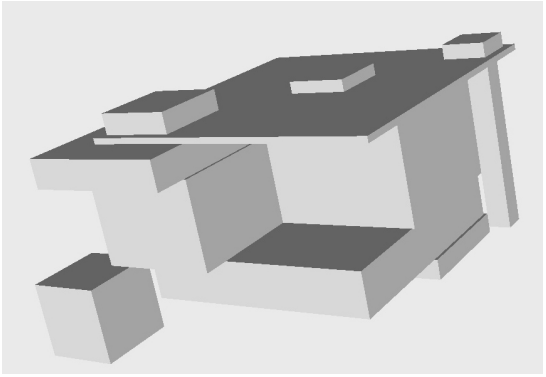

(d) Model of hummock.

Figure 9: Schematic presentation of models with hummock.

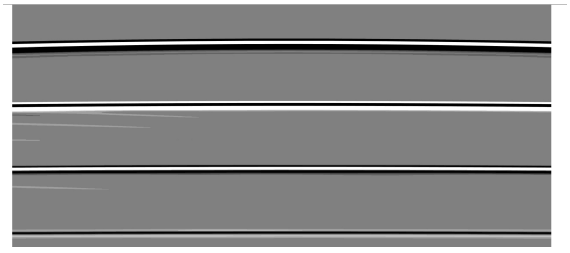

(a) Model with hummock and without oil and gas layer.

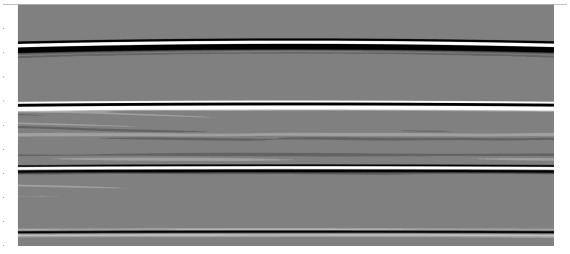

(b) Model with hummock and oil and gas layer.

(c) Model without hummock and oil and gas layer.

Figure 10: Typical seismograms to distinguish the situations of presence and absence of the oil and gas layer and hummock.

The z-axis seismograms for these formulations of the problem are presented in Fig. 10. Figures 10a and 10b show that the hummock does not contribute essentially into seismograms, the reflections from the water and soil layers are clearly seen. In contrast with Fig. 10a, the additional reflections from the oil and gas layer are seen in Fig. 10b. There is no response from the left in Fig. 10c because this model does not contain the hummock.

7 Conclusions

1. A grid-characteristic method has been developed for numerical solution of direct seismic exploration problems in Arctic.
2. Using the grid-characteristic method, numerical experiments solving seismic exploration problems on Arctic shelf were carried out. The corresponding seismograms were constructed for each formulation of the problem, the responses from media with different densities and speed of sound (ice, water, soil, oil and gas layer) were analyzed in detail.
3. For these formulations of the problem the seismograms presented in the paper show that ice formations do not give essential responses in the direction perpendicular to the sea surface. This conclusion is in good agreement with the results of studies undertaken under real conditions [3].
4. The calculations show the efficiency of the grid-characteristic method for numerical solution of direct problems of seismic exploration in the Arctic.

Funding: The work was supported by the Russian Science Foundation (project No. 14–11–00434).

References

[1] D. Averna and E. Tornatore, Ordinary $(p_1, \ldots, p_m)$-Laplacian systems with mixed boundary value conditions, *Nonlinear Analysis: Real World Applications* **28** (2016), 20–31.
[2] A. T. Bekker, O. A. Sabotash, V. I. Seliverstov, G. I. Koff, and E. N. Pipko, Estimation of limit loads on engineering offshore structures. In: *Int. Soc. Offshore and Polar Eng.*, The Nineteenth Int. Offshore and Polar Eng. Conf., July 21–26, 2009, Osaka, Japan, pp. 574–579.
[3] S. J. Betterly, M. A. Speece, R. H. Levy, D. M. Harwood, and S. A. Henrys, A novel over-sea-ice seismic reflection survey in McMurdo Sound, Antarctica. *Terra Antarctica* **2** (2007), No. 14, 97–106.
[4] C. Chapman, *Fundamentals of Seismic Wave Propagation*, Cambridge University Press, 2004.
[5] S. E. Donskoi, *The report of the Minister of Nature Resources and Ecology of the Russian Federation*. Scientific-technical problems of opening up the Arctic, 2014, pp. 8–13.
[6] A. V. Favorskaya, D. I. Petrov, N. I. Khokhlov, and I. B. Petrov, Numerical solution of elastic-acoustic problems with the help of grid-characteristic method. *Vestnik IKBFU* (2015), No. 10, 7–12.
[7] L. Yu. Frolenlova, V. S. Shorkin, and S. I. Yakushina, Version approach to the modelling of linear elastic medium. *News of the Tula State University. Natural Sciences* **2** (2013), No. 2, 284–296 (in Russian).
[8] S. V. Frolov, V. E. Fedyakov, V. Yu. Tret'yakov, A. E. Klein, and G. V. Alekseev, New data on change in ice thickness in the Arctic Ocean. *Doklady Earth Sciences* **425** (2009), No. 1, 104–108.
[9] R. V. Goldstein and N. M. Osipenko, Crack resistance and destructions of ice cover by ice-breakers. *AANII Transactions* **391** (1986), 137–156.
[10] R. V. Goldstein and N. M. Osipenko, Fracture mechanics of ice and some its applications. *Sib. J. Pure Appl. Math.* **12** (2012), No. 4, 41–47.
[11] V. I. Golubev, I. B. Petrov, and N. I. Khokhlov, Numerical simulation of seismic activity by the grid-characteristic method. *Comp. Math. Math. Phys.* **53** (2013), No. 10, 1523–1533.
[12] D. P. Grigorievykh, N. I. Khokhlov, and I. B. Petrov, Mathematical modelling of cracks in solid deformable bodies using hexahedral grids. *MIPT Trans.* **7** (2015), No. 4, 28–37 (in Russian).
[13] N. I. Khokhlov and I. B. Petrov, Modelling of seismic events by grid-characteristic method. *MIPT Trans.* **3** (2011), 159–167 (in Russian).
[14] A. S. Kholodov and Ya. A. Kholodov, Monotonicity criteria for difference schemes designed for hyperbolic equations. *Comp. Math. Math. Phys.* **46** (2006), No. 9, 1560–1588.
[15] A. A. Kucheiko, A. Yu. Ivanov, A. A. Davydov, and A. Yu. Antonyuk, Iceberg drifting and distribution in the Vilkitsky Strait-studied by detailed satellite radar and optical images. *Izvestiya, Atmospheric and Oceanic Phys.* **52** (2016), No. 9, 1031–1040.
[16] I. E. Kvasov, S. A. Pankratov, and I. B. Petrov, Numerical simulation of seismic responses in multilayer geologic media by the grid-characteristic method. *Math. Models Comp. Simul.* **3** (2011), No. 2, 196–204.
[17] S. G. Lee, S. H. Juhand, and G. Y. Kong, Modelling and simulation system for marine accident cause investigation. In: *Collision and Graunding of Ships and Offshore Structures* (Eds. J. Amdahl, S. Ehlers, and J. Leira). Taylor and Francis Group, London, 2013, pp. 39–47.

[18] B. V. Leer, Towards the ultimate conservative difference scheme, III. Upstream-centered finite-difference schemes for ideal compressible flow. *J. Comp. Phys.* **23** (1977), No. 3, 263–275.
[19] X. Lin and X. Yu, A finite difference method for effective treatment of mild-slope wave equation subject to non-reflecting boundary conditions. *Applied Ocean Research* **53** (2015), 179–189.
[20] A. E. H. Love, *A Treatise on the Mathematical Theory of Elasticity*. Courier Corporation, 1944.
[21] K. M. Magomedov and A. S. Kholodov, *Grid-Characteristic Numerical Methods*. Nauka, Moscow, 1988 (in Russian).
[22] A. Marchenko, Thermodynamic consolidation and melting of sea ice ridges. *Cold Regions Science and Technology* **52** (2008), No. 3, 278–301.
[23] W. Novacki, *Theory of Elasticity*. Mir, Moscow, 1975 (in Russian).
[24] I. B. Petrov, Influence of ice and water on offshore structures and coastal zones of the Arctic. Russian Academy of Sciences. *Scientific-technical Problems of Opening up the Arctic*, Scientific session of the General meeting of members of the RAS, December 16, 2014.
[25] I. B. Petrov, A. V. Favorskaya, I. E. Kvasov, and A. V. Sannikov, The methodology of representation and interpretations of the results of fullwave seismic calculations. *MIPT Trans.* **6** (2014), No. 1, 154–161 (in Russian).
[26] I. B. Petrov, A. V. Favorskaya, A. V. Sannikov, and I. E. Kvasov, Grid-characteristic method using high-order interpolation on tetrahedral hierarchical meshes with a multiple time step. *Math. Models Comp. Simul.* **25** (2013), No. 5, 409–415.
[27] I. B. Petrov and N. I. Khokhlov, Modelling 3D seismic problems using high-performance computing systems. *Math. Models Comp. Simul.* **6** (2014), No. 4, 342–350.
[28] I. B. Petrov, M. V. Muratov, A. V. Favorskaya, V. A. Biryukov, and A. V. Sannikov, Numerical modelling of straight 3D exploration seismology problems with the use of grid-characteristic method on unstructured tetrahedral meshes. *Computer Research and Modelling* **7** (2015), No. 4, 875–887.
[29] L. Strub-Klein and D. Sudom, A comprehensive analysis of the morphology of first-year sea ice ridges. *Cold Regions Science and Technology* **82** (2012), 94–109.
[30] K. S. Yee, Numerical solution of initial boundary value problems involving Maxwell's equations in isotropic media. *IEEE Trans. Antennas Propagation* **14** (1966), No. 3, 302–307.
[31] Q. Zhou and P. J. Diamessis, Lagrangian flows within reflecting internal waves at a horizontal free-slip surface. *Physics Fluids* **27** (2015), No. 12, 126601–126601.15.